Electrochimica Acta 324 (2019) 134780

Contents lists available at ScienceDirect

Electrochimica Acta

journal homepage: www.elsevier.com/locate/electacta

Electrochemical gas phase oxidation of hydrogen chloride to chlorine: Model-based analysis of transport and reaction mechanisms

Simon Bechtel [a], Antonio Sorrentino [b], Tanja Vidaković-Koch [b], Adam Z. Weber [c], Kai Sundmacher [a, d, *]

[a] Max Planck Institute for Dynamics of Complex Technical Systems, Department Process Systems Engineering, Sandtorstr.1, D-39106, Magdeburg, Germany
[b] Max Planck Institute for Dynamics of Complex Technical Systems, Department Electrochemical Energy Conversion, Sandtorstr.1, D-39106, Magdeburg, Germany
[c] Energy Conversion Group, Energy Technologies Area, Lawrence Berkeley National Laboratory, 1 Cyclotron Road, Berkeley, CA, 94720, USA
[d] Otto-von-Guericke- University Magdeburg, Department Process Systems Engineering, Universitätsplatz 2, D-39106, Magdeburg, Germany

ARTICLE INFO

Article history:
Received 9 July 2019
Received in revised form
26 August 2019
Accepted 28 August 2019
Available online 31 August 2019

Keywords:
Gas phase oxidation
Hydrogen chloride oxidation
Chlorine production
Reaction-limited current
Numerical reactor model

ABSTRACT

The electrochemical conversion of hydrogen chloride to chlorine plays a significant role within major industrial processes like the polyurethane or polycarbonate production. Our recent studies demonstrated that the direct electrolysis of gaseous HCl in combination with novel strategies for product purification leads to significant exergetic savings (36–38%) compared to the Bayer UHDENORA state-of-the art process, which employs aqueous hydrochloric acid as a feedstock. Furthermore, we showed that despite of the improvements in the efficiency of the electrochemical reactor, it still has by far the greatest exergy demand of all process units. While the oxygen depolarized cathode (ODC) utilized in both process variants has been investigated in great detail in the scientific literature, the oxidation reaction of gaseous HCl (HClOR) has not yet received much attention and is hence the major subject of this work. In earlier experimental investigations of the HClOR, a limiting current was observed that has the potential to critically reduce the performance of the overall reactor. In the past, membrane dehydration and mass transfer resistances on the anode side were suggested as possible reasons. In order to shed light on this phenomenon, a dynamic, one dimensional agglomerate model of the gas phase HCl oxidation half-cell, considering detailed micro kinetics, as well as the mass transfer of HCl in the different cell parts, is developed. The modeling results suggest that neither mass transfer resistance nor membrane dehydration but a kinetic limitation is the underlying reason for the observed limiting behavior. This has a significant impact on the strategy for further reactor optimizations and harbors the potential of major energy savings in an industrial application of this highly relevant process.

1. Introduction

Chlorine is a base chemical employed in the production of plastics, solvents and various other chemical compounds [1,2], with a production capacity of 66 million tons worldwide in 2014, which is expected to increase to up to 76 million tons per year until 2019 [3]. One third of all substances produced with the aid of chlorine do not contain Cl_2 themselves and 50% of the used chlorine is being discharged in the form of side products like hydrogen chloride or chloride salts [4]. Example processes with a further growing industrial relevance are the isocyanate and polycarbonate production in which HCl emerges as a side product [1,4,5]. Hydrogen chloride consuming processes, like the production of PVC, are growing at a much slower rate. Hence, the market for this byproduct is oversaturated [4,5]. For this reason, various processes for the electrochemical and heterogeneously catalyzed conversion of hydrogen chloride to chlorine have been industrially employed (see Ramirez et al. [4] and Bechtel et al. [6]).

The most efficient industrially employed process for the electrolysis of HCl is the Bayer UHDENORA process, in which aqueous hydrochloric acid is converted to chlorine [6,7]. As our group recently showed [6], utilizing a gas phase reactor as proposed by Martínez et al. [7] and Kuwertz et al. [8] in combination with novel

* Corresponding author. Max Planck Institute for Dynamics of Complex Technical Systems, Department Process Systems Engineering, Sandtorstr.1, D-39106, Magdeburg, Germany.
E-mail address: Sundmacher@mpi-magdeburg.mpg.de (K. Sundmacher).

https://doi.org/10.1016/j.electacta.2019.134780

product purification strategies leads to exergetic savings of 38% on the overall process level. A further result of this work was the insight that more than 90% of the exergy demand of the gas phase process is related to the electrochemical reactor and only less than 10% to the subsequent separation of unreacted HCl and chlorine [6]. Hence, to further increase the efficiency of this novel process, a better understanding of the gas-phase reactor and the utilization of this knowledge for a systematic reactor optimization is critical. Similar to the liquid-phase reactor, the gas-phase reactor also employs an oxygen depolarized cathode (ODC) in order to reduce the overall energy demand. While Kuwertz et al. [9] demonstrated that also in the gas phase reactor the ORR contributes most to the overpotential of the cell at the investigated current densities of up to 400 mA cm^2, it has been studied extensively in the scientific literature already in the frame of various kinetic and PEM fuel cell studies [10–13], contrary to the anodic gas phase oxidation of HCl. Experimental investigations of the HClOR [14–16] show a comparably low overpotential of less than 200 mV at intermediate current densities (100–400 mA/cm^2). However, all of these studies display the phenomenon of a limiting current in the range of 400–900 mA/cm^2, which so far is not satisfactorily understood and explained in the scientific literature. At higher, yet still technically relevant current densities, the HClOR therefore becomes of great significance, as it has the potential to limit the performance of the overall gas-phase reactor. The present work therefore focusses on the HClOR in order to investigate and explain the experimentally observed limiting behavior and to propose possible optimization strategies.

Historically, the first investigations of the gas-phase oxidation of HCl stem from Trainham et al. [14], which resulted in a patent by Dupont. Their reactor differs from the one developed by Kuwertz et al. [8] in regards to the cathodic reaction, where hydrogen is emerging in the case of the Dupont reactor. While their experiments already exhibited the above mentioned limiting behavior, it was not further discussed. The first attempt in this direction was made by Eames et al. [15], who developed a simplified numerical model of the HClOR. They predicted the experimentally observed limiting behavior to be due to a dehydration of the membrane adjacent to the anode catalyst layer (ACL) and the corresponding strong increase in its ohmic resistance. However, they did not consider the transfer of water from the cathode chamber, which was filled with liquid water, through the membrane into the anode chamber of the reactor. Since no water transfer into the ACL is included in their model, the best performance, meaning a higher reaction limited current before membrane dehydration starts to manifest, is obtained in simulations at the highest reactor temperature. This is due to the slight increase in the diffusion coefficient of water in the membrane leading to a faster mass transfer from the cathode to the anode side, delaying membrane dehydration. However, as is well known from PEM fuel-cell studies [17,18], higher temperatures actually facilitate the dehydration of the membrane due to an increasing flux of water leaving the membrane towards the anode chamber. If the limiting behavior was indeed a consequence of membrane dehydration, one would therefore expect lower limiting current densities when increasing the temperature, which contradicts the experimental results of Trainham [14], Eames [15] and Martínez [16].

Hence, while the model of Eames et al. [15] is, after some adjustments to the diffusion coefficient of water in Nafion, able to reproduce the experimentally observed limiting behavior, a consideration of the underlying physics indicate that the model is incomplete and that the limiting behavior is most likely not a consequence of membrane dehydration. This is underlined by recent experimental investigations of the HClOR half-cell reaction by Martínez et al. [16,19,20], who corrected their measurements for ohmic drop. A limiting current similar to the one measured by Eames et al. [15] and Trainham et al. [14] was observed nonetheless, even though no ohmic resistance of the membrane was included. Martínez et al. seemingly attributed this effect to mass-transfer limitations on the anode side, as can be deduced from their significant correction of Tafel plots for mass-transfer resistance, as further discussed in chapter 3. To investigate this hypothesis and shed light on the phenomenon of the observed limiting current, a dynamic one-dimensional isothermal agglomerate half-cell model of the HClOR is developed in the present work and validated against experimental results from Martínez et al. [20] at two different temperatures. A focus is put on describing the mass transfer of the involved gas species in the GDL and in the agglomerates of the catalyst layer in order to determine whether the experimentally observed limiting behavior is indeed a consequence of slow mass transfer. Furthermore, a microkinetic reaction scheme of the HClOR including the adsorption of the chloride species on the platinum surface is considered instead of the macrokinetic Butler-Volmer approach employed by Eames et al. [15] or the simplified kinetic expression proposed by Martínez et al. [20], in order to realistically evaluate the influence of the reaction kinetics on the limiting behavior of the HClOR.

In section 2 of the present work, the underlying assumptions of the reactor model as well as all relevant governing equations and boundary conditions are delineated. Section 3 consists of a discussion of the reaction mechanism and its impact on the experimentally observed limiting behavior as well as the role of mass transfer resistances in the gas diffusion media and the agglomerates of the catalyst layer. Based on these insights, reactor optimization strategies and their potential impact on the energy demand of an industrial example plant are discussed.

2. Model

A scheme of the electrochemical reactor, as investigated in the experiments of Martínez et al. [16,19,20] towards which the conditions in simulations in the present work were adapted to, is shown in Fig. 1. Since the measurements by Martínez et al. [16,19,20] were carried out in a half-cell and his polarization curves are expressed on the scale of a reference hydrogen electrode, the here presented numerical model includes only the processes related to the working electrode (anode) and the membrane, while the counter electrode processes are excluded.

Assumptions:

- All gases are treated as ideal gases and the reactor is assumed to be isothermal due to the maximum conversion being less than 5% and the circulation of sulfuric acid through the cathode chamber.
- Water in the anode compartment of the cell is assumed to be in its gaseous state only.
- The membrane is modeled as impermeable for all species besides water and protons.
- The gaseous HCl is absorbed and dissociates within the water containing agglomerates of the catalyst layer. Hence the expressions for the reaction kinetics are based on the activity of the aqueous Cl^- species.

In the following subsections, the governing equations for each layer, as depicted in Fig. 1, are explained. The simulations were carried out for temperatures of 40 °C and 60 °C, to validate the ability of the model to correctly predict the experimentally observed temperature dependence of the reactor performance in the work of Martínez et al. [20].

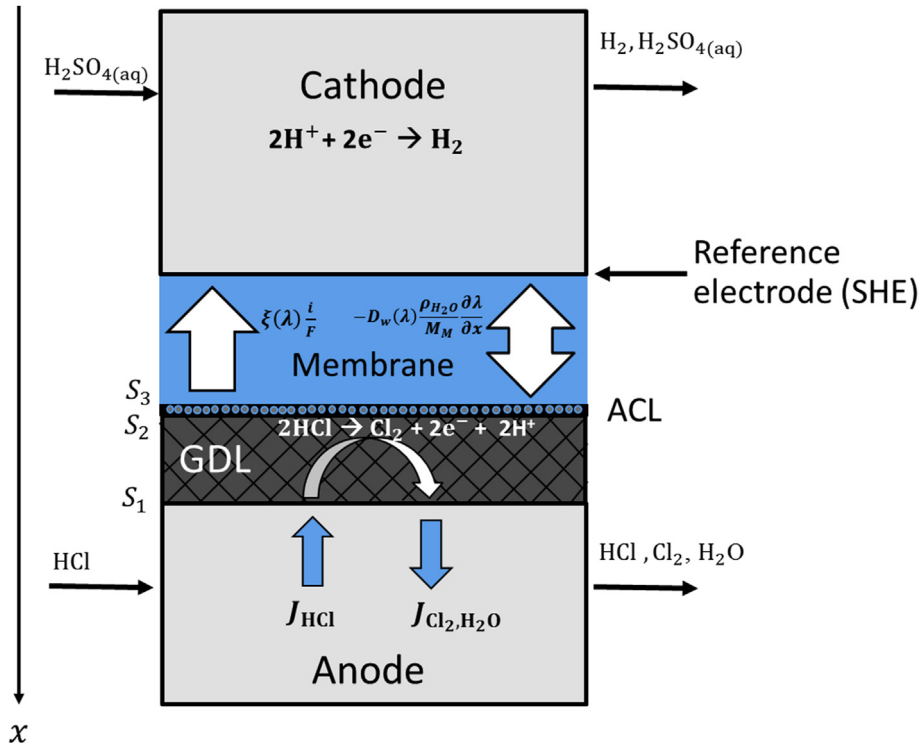

Fig. 1. Scheme of the electrochemical half-cell reactor including the underlying physical processes taking place in the gas phase electrolysis of HCl to chlorine.

2.1. Mass balance in the gas channel and the gas diffusion layer (GDL)

The gas channels of the volume V are assumed to be perfectly mixed, meaning that the gas composition within the gas anode chamber is identical to the composition of the outlet gas stream. In addition to the convective mass flux, a source or sink term $J_i|_{S1,t}$, considering the anodic oxidation reaction and the crossover of water through the membrane into the anode chamber, is included. The change of the partial pressures of all species within the gas anode chamber P_i^{GC} can hence be described by equation (1):

$$V\frac{dP_i^{GC}}{dt} = \left(\dot{V}_{in}P_{i,in}^{GC} - \dot{V}_{out}P_i^{GC}\right) + RTJ_i|_{S1,t} \tag{1}$$

where $\dot{V}_{in}$ and $\dot{V}_{out}$ describe the volumetric flow rate entering and leaving the reactor respectively. Based on the experimental setup of Martínez et al. [16], the outlet pressure of the reactor, and hence the pressure in the gas anode chamber P_{tot}^{GC}, can be assumed to be approximately 1 bar. Hence, under consideration of the electrochemical reaction and the crossover of water, the reactor outlet flow rate can be calculated as follows:

$$\dot{V}_{out} = \dot{V}_{in} + \frac{RT}{P_{tot}^{GC}}A_{surf}\left(J_{HCl}|_{S1,t} + J_{Cl_2}|_{S1,t} + J_{H_2O}|_{S1,t}\right) \tag{2}$$

The electrode area A_{surf} was set to a value of 2.3 cm^2 based on the experiments of Martínez et al. [20]. The diffusive mass transport in the GDL is modeled employing the inverted solutions of the Maxwell-Steffan equations and the convective flux by employing Darcy's law for $n-1$ species.

$$\frac{\partial P_i^{GDL}}{\partial t} = -\nabla\left[\frac{P_{tot}^{GDL}}{RT}\sum_{j\neq i}\overline{D_{ij}}_{eff}\nabla\frac{P_j^{GDL}}{P_{tot}^{GDL}}\right] - \frac{k_{eff,g}}{\mu_g}\nabla\left(P_i^{GDL}\nabla P_{tot}^{GDL}\right) \tag{3}$$

Due to the large pores in the diffusion media employed in the experiments of Martínez and Kuwertz [9], Knudson diffusion has a negligible impact on the diffusive mass transfer. As determined by Kuwertz et al. [9], 19.2% of the pores had a radius of approximately 100 µm, 49% a pore radius of 10 µm and 31.8% a pore radius of 25 nm. Simulating the diffusive mass transport based on the Dusty Gas model [21] according to equations (4) and (5) showed deviations of less than 0.1% compared to the classical Maxwell-Steffan equations. This is in agreement with experimental investigations of mass transfer in porous diffusion media by Spingler et al. [22].

$$\nabla x_i = \sum_{j=1}^{3}\frac{N_i x_j - N_j x_i}{D_{ij}^{eff}} + \frac{N_i}{D_{iM}^{eff}} \tag{4}$$

Here, the effective Knudsen diffusion coefficient is denoted as D_{iM}^{eff} and calculated as follows, employing again the Bruggeman correlation.

$$D_{iM}^{eff} = \varepsilon_{GDL}^{1.5}\frac{\int rV(r)dr}{3}\sqrt{\frac{8RT}{\pi M_i}} \tag{5}$$

For this reason, equation (3), employing the classical Maxwell-Steffan approach, was used to describe the mass transfer within the diffusion media in the presented model. The partial pressure of the n-th species is calculated based on the fact that the sum of all partial pressures must be equal to the total pressure determined by Darcy's law:

$$\sum_i P_i^{GDL} = P_{tot}^{GDL} \tag{6}$$

$$\frac{\partial P_{tot}^{GDL}}{\partial t} = \nabla\left(-\frac{P_{tot}^{GDL} k_{eff,g}}{\mu_g} \nabla P_{tot}^{GDL} \right) \tag{7}$$

The viscosity of the overall mixture μ_g was assumed to be identical to the viscosity of pure gaseous HCl μ_{HCl} since this component makes up for approximately 80–90% of the gas mixture under all conditions investigated in this work. The effective diffusion coefficients are calculated based on the Bruggeman correlation,

$$\overline{D_{ij}}_{eff} = \overline{D_{ij}} \varepsilon^{1.5} \tag{8}$$

where ε is the porosity of the layer. More detailed information on the determination of the diffusion coefficients $\overline{D_{ij}}$ are given in the supplemental information of this work and in Refs. [23,24].

2.2. Mass balance and proton conductivity in the Nafion membrane

The water content of the membrane λ_W is defined as

$$\lambda_M = c_W \frac{E_M}{\rho_M} \tag{9}$$

where c_W is the concentration of water in the Nafion membrane, ρ_M is the density of the dry membrane and *EW* its equivalent weight. Martínez et al. [16,19,20] used a Nafion 117 membrane in their experiments. Hence, the membrane thickness employed in the numerical model is 178 µm. The dynamic balance of the water content can be formulated as follows [25]:

$$\frac{\partial \lambda_M}{\partial t} = -\frac{\partial N_W}{\partial x} \frac{M_W}{\rho_W} \tag{10}$$

$$N_W = -D_W(\lambda_M) \frac{\rho_M}{M_M} \frac{\partial \lambda_M}{\partial x} - \xi(\lambda_M) \frac{i}{F} \tag{11}$$

Here, $\xi(\lambda_M)$ is the osmotic drag coefficient, which is a function of the water content and the drag constant K_M according to equation (12). The water flux consists of three components: A diffusive flux due to the activity gradient of water along the sandwich coordinate perpendicular to the MEA surface, an electroosmotic flow due to the protons migrating from anode to cathode dragging water molecules with them and lastly a hydraulic flux which originates in the capillary pressure gradient along the sandwich coordinate. According to Eikerling et al. [26], the diffusive and hydraulic flux can be summarized and described together by an effective diffusion coefficient D_W. The authors are aware that employing the gradient in the water content instead of the chemical potential as a driving force is less accurate from a physical point of view. However, as delineated in the course of this section, this approximation is of little influence to the objectives of the present work and in addition, this model proved to be reasonably reliable in for example the work of Sorrentino et al. [25].

Zawodzinski et al. [27] have proposed a value of 2.5 for the osmotic drag coefficient in a fully hydrated Nafion membrane in contact with water. However, in the case of the HClOR, the influence of hydrogen chloride on the transport coefficients has to be considered [28,29]. Motupally et al. [29] experimentally determined a value of 3.5 for the osmotic drag coefficient at a temperature of 60 °C in their set up of the gas phase electrolysis of HCl. They assumed that a thin liquid film will form on the ACL due to exergonic reaction of water and HCl leading to the condensation of parts of the water crossing over through the membrane from the cathode side. Hence, their osmotic drag coefficient was determined in a setup where the membrane supposedly is in equilibrium with water on the cathode side and hydrochloric acid on the anode side.

While in the present work, all water in the anode chamber of the reactor is presupposed to be in its gaseous state, HCl is considered to absorb in the agglomerates of the catalyst layer, as mentioned in the model assumptions in section 2.1. Hence, also in the present work the membrane can to a certain extent be expected to be in contact with condensed hydrochloric acid in the ACL so that the value for the drag coefficient determined by Motupally et al. [29] seems to be a reasonable choice for the here presented model. However, Motupally et al. [29] assumed a maximum water content of 22 for the Nafion membrane, due to its contact with water on the cathode side of their reactor, which they base on experimental findings of for example Zawodzinski et al. [27]. In the experiments of Martínez et al. [16,19,20] however, the cathode chamber is filled with dilute sulfuric acid. According to Tang et al. [30], the approximate water content of a Nafion 117 membrane equilibrated with 1 M H_2SO_4 is 17. Hence, assuming a linear relationship between drag coefficient and water content as for example done by Ref. [25], the maximum drag coefficient of the fully hydrated membrane in Martínez' setup is calculated to be $17/22 \cdot 3.5 = 2.7$. For any other given water content λ_M below the equilibrium value of 17, the drag coefficient is calculated accordingly:

$$\xi(\lambda_M) = K_M \lambda_M = \frac{2.7}{17} \lambda_M \tag{12}$$

The Fickian diffusion coefficient of water in Nafion in equation (11) can be described according to an empirical equation by Fuller et al. [31]. To account of the presence of HCl, Motupally et al. proposed an expression, which additionally considers the influence of hydrochloric acid on the dependence between water activity and water content within the membrane, as displayed in equation (14):

$$D_W(\lambda_M) = \lambda_M D_W^0 e^{-\frac{2436}{T}} \tag{13}$$

$$D_W(\lambda_M)_{HCl} = D_{W,I}(\lambda_M)_{HCl} \frac{\partial \ln(aW)}{\partial \ln(\lambda_M)} = \frac{1.96 \cdot 10^{-7} \lambda_M (\lambda_M - 0.0209\lambda_M^2 - 0.501)}{\lambda_M - 2} e^{-\frac{2436}{T}} \tag{14}$$

For reasons discussed in detail in the supporting information, the model proposed by Fuller [31] as depicted in equation (13) instead of equation (14) by Motupally [29] is employed in the present work. In future investigations, the effect of gaseous hydrogen chloride on the diffusion coefficient of water in Nafion should be investigated in a consistent and rigorous way to reduce the uncertainties in describing the water transport through the membrane within a hydrogen chloride gas phase electrolyzer.

Since the experiments by Martínez et al. [16,19,20], towards which the model is validated, are corrected for ohmic resistance, the potential losses the membrane are of little relevance for the present model. However, in order to be able to employ the model in settings where the ohmic resistance is considered, it is nonetheless calculated although not actively used in the here presented simulations. Again it has to be considered that, just as the above mentioned transport coefficients, also the ionic conductivity of the membrane is influenced by the presence of HCl [28]. However, in order to include this effect, measurements of the ionic conductivity at different water contents in the membrane in presence of gaseous hydrogen chloride are needed. The interval of measured water

contents should also include the equilibrium values for a membrane in contact with water vapor and not only liquid water or acid, since the water vapor pressure in the anode compartment is below its saturation pressure. This data however is not available in the scientific literature. Therefore, it is assumed that the ionic conductivity of Nafion membranes will not be significantly influenced by the presence of gaseous HCl and can be described with equation (15) by Springer et al. [32], which was developed for the presence of pure water only.

$$\kappa_M = (0.005139\lambda_M - 0.00326)e^{1268\left(\frac{1}{303}-\frac{1}{T}\right)} \tag{15}$$

The potential loss in the membrane can then be calculated according to equation (16) [25]. This treatment slightly underestimates the potential loss, since the contribution of the osmotic drag of water molecules through the membrane is not accounted for as for example done in Ref. [33]. If a more precise determination of the potential profile in the membrane is desired, this contribution can be added to equation (16).

$$\Delta\Phi_M = i\int_0^{d_M}\frac{dx}{\kappa_M(\lambda_M)} \tag{16}$$

Overall, the presence of gaseous HCl introduces various uncertainties due to its influence on the transport properties within the membrane, which only to a certain extent can be accounted for utilizing the experimental data of Motupally et al. [29,34] and Balko et al. [35]. Since the purpose of this work is to explain the experimentally observed limiting behavior and furthermore, since no ohmic contributions are considered, the remaining uncertainties and approximations made have little impact on the presented results.

2.3. Catalyst layer and electrochemical reaction

On the macroscale level, the catalyst layer is modeled in steady-state and as an interface, since studies of PEM fuel cells imply that the gas phase concentration of the reactants in a thin catalyst layer are almost spatially constant [36]. Furthermore, as explained in section 3.2 of this work, small variations in the gas phase concentration of HCl have very little impact on the activity of the dissolved $HCl_{(aq)}$ in the Nafion of the catalyst layer. The macroscale of the catalyst layer can hence be described in the form of a boundary condition as shown in section 2.4. On the microscale level however, an agglomerate model was employed, to model the interaction between mass transfer and kinetics within the agglomerates accurately.

The following reaction network, where dissolved chloride anions instead of gaseous HCl are assumed to be the reacting species, as discussed in the assumptions at the beginning of this section, was employed to derive an expression for the overall reaction rate:

$$Cl^- + Pt \leftrightharpoons PtCl + e^- \tag{17}$$

$$2PtCl \leftrightharpoons 2Pt + Cl_{2\,(g)} \quad (A) \tag{18}$$

$$Cl^- + PtCl \leftrightharpoons Pt + Cl_{2\,(g)} + e^- \quad (B) \tag{19}$$

This mechanism is identical to the one proposed for the electrolysis of brine [37]. Even though the chemical nature of the system, pH and reactant concentration differs clearly, the presence of chloride anions in both systems is a common foundation, and hence distinct works in the field of the kinetics of the brine electrolysis shall be mentioned shortly: Depending on the catalyst system and the experimental conditions, there are various works that assumed the Tafel step A to be predominant over the electrochemical step B and to limit the overall reaction rate [38,39] while other investigations showed the step B to be predominant and rate limiting [37]. For the sake of completeness, it should be mentioned that for the brine electrolysis a third possible mechanism, the chloronium ion pathway, was suggested [37,40,41]. In the present work considering the HClOR, step A is assumed to be predominant and rate limiting based on a reevaluation of the experimental data from Martínez et al. [16,19,20], as explained in section 3.1 of the present work, in which the following equation for calculating the current density on the microscale j^μ is derived in detail:

$$j^\mu = 2Fk_A\left(\frac{K_0 a^\mu_{Cl^-}}{1+K_0 a^\mu_{Cl^-}e^{\frac{F\eta_A}{RT}}}\right)^2 e^{\frac{2F\eta}{RT}}\left(1-e^{\frac{-2F\eta_A}{RT}}\right) \tag{20}$$

Hereby k_A is the rate constant of the Tafel step, $a^\mu_{Cl^-}$ stands for the activity of chloride anions within the agglomerates, and K_0 represents the equilibrium constant for the adsorption and desorption of chloride anions on the platinum surface according to equation (17).

Employing the rate expression in equation (20), the flux ag^μ_i of species i into and out of the agglomerate can be calculated according to equation (19), which only has to be solved for the species $HCl_{(aq)}$, since the according flux for chlorine directly follows from the stoichiometry of the reaction: $ag^\mu_{HCl_{(aq)}} = -2ag^\mu_{Cl_2}$

$$ag^\mu_i = -\frac{1}{R^2}a\int_{r=0}^{r=R} r^2 a^\mu r^\mu(a^\mu_i,\eta_A)dr \tag{21}$$

In equation (21), R is defined as the radius of the agglomerates, a the ratio of the agglomerate surface to its volume, r^μ the reaction rate on the microscale, a^μ the specific internal area of the agglomerates and a^μ_i the activity of the species i within the agglomerate. The radius of the agglomerates in the experiments of Martínez et al. [20] is not precisely known. Hence, a literature value of 200 nm proposed by Ref. [42] is chosen, instead of treating the agglomerate size as a fit parameter, in order to obtain physically feasible and realistic results and not simply enhance the accuracy of the model with an increased amount of fitting parameters. It should be noted that there are also various literature sources assuming greater radii [43,44] as well as smaller radii [45], hence in 3.2 the influence of the agglomerate size on the presented results is investigated and discussed in more detail.

To solve equation (21), the activity of Cl^- anions within the agglomerate $a^\mu_{Cl^-}$ as a function of the spatial coordinate r must be determined by solving the mass balance on the microscale, where $\upsilon_{Cl^-} = -2$ is the stoichiometric coefficient for the chloride anions in the global reaction scheme:

$$\frac{\partial c^\mu_{Cl^-}}{\partial t} = -\frac{1}{r^2}\frac{\partial}{\partial r}\left(r^2 D^{\mu,eff}_{HCl_{(aq)}-H_2O}\frac{\partial c^\mu_{Cl^-}}{\partial r}\right) + a^\mu \upsilon_{Cl^-} r^\mu\left(a^\mu_{Cl^-},\eta_A\right) \tag{22}$$

For first-order reactions and constant activity coefficients, an analytical solution of equation (22) is available that is widely used in the scientific literature for modeling the ORR in PEM fuel cells [21]. In the present work, however, this equation has to be solved numerically, since a more complex expression for the reaction rate is employed and because not only the concentration but also the activity coefficient of the chloride anions is a function of the spatial coordinate.

Please note, that the diffusive flux is described by Fick's law, assuming a two component system of water and $HCl_{(aq)}$. Since the equilibrium mole fraction of Cl_2 in water at 60 °C is only 0.00094 at a vapor pressure of 1.013 bar, its influence on the diffusion of $HCl_{(aq)}$ in water can be neglected. The composition dependence of the diffusion coefficient $D^{\mu,eff}_{HCl_{(aq)}-H_2O}$ in Nafion is not known. Hence, a constant value from the work of [28] is employed. As further explained in section 3.3, this appears to be a reasonable approximation.

The charge balance for the double layer of anode is formulated with the electrode double layers acting as a capacitor and the charge transfer acting as an ohmic resistance in parallel.

$$j = C_{DL}\frac{d\eta_A}{dt} - L_{ACL}ag^{\mu}_{HCl_{(aq)}}F \tag{23}$$

where C_{DL} is the capacity of the double layer and L_{ACL} the catalyst layer thickness. The overall electrode potential E is calculated as

$$E = E_{OCP} - \eta_A \tag{24}$$

2.4. Boundary conditions

Due the presence of HCl, chlorine and water in the anode GDL, 3 s-order partial differential equations (PDEs) have to be solved, two for the individual mass balances for HCl and chlorine and one for the overall mass balance. Together with the PDE that describes the water transport in the membrane, and the one for the mass balance of chloride anions in the agglomerates, this leads to the need for 10 boundary conditions.

At the interface between the gas channel and the GDL (interface S_1 in Fig. 1), continuity of the partial pressure of each substance is assumed; the overall pressure at this interface is set to 1 bar. The continuity of pressures is also chosen as a boundary condition for the GDL/CL interface S_2 for which the partial pressures of all species in the catalyst layer can be obtained based on equations (26) and (27).

$$p^{GDL}_i|_{x=S_1,t} = p^{GC}_i \; and \; p^{GC}_{tot} = 1 \; bar \tag{25}$$

Since the catalyst layer is treated as an interface, the flux of a species entering and leaving the layer, calculated based on equation (21), multiplied with its thickness is equivalent to the source or sink terms within the layer. Hence, for the reacting species HCl and Cl_2

$$J_i|_{x=S_2,t} = L_{ACL}ag^{\mu}_i \tag{26}$$

For the overall mass balance, the convective flux at this boundary, calculated based on Darcy's law, is set equal to the source sink terms already included in equation (26) in addition to the flux of water through the membrane by means of diffusion and electroosmotic drag, all being summarized in the term s_{tot}.

$$\left(\frac{p_{tot}k_{eff,g}}{\mu_g}\nabla p_{tot}\right)\Big|_{x=S_2,t} = s_{tot} \tag{27}$$

Furthermore, equilibrium between water in the gas phase and the water content λ_{CL} on the catalyst interface is assumed. For this purpose, the isothermal water uptake equation from Springer et al. [32] is employed. Since the present work only investigates the HClOR and not the cathodic reaction, a value of $\lambda_{CCL} = 17$ was fixed for the membrane interface towards the cathode side of the cell. As discussed in section 2.2, this is the approximate water content of a Nafion 117 membrane equilibrated with 1 M H_2SO_4.

$$\lambda_{ACL} = 0.043 + 17.81\frac{P^{ACL}_{H_2O}}{P_{sat}}\Big|_{x=S_i,t} - 39.85\frac{P^{ACL}_{H_2O}}{P_{sat}}\Big|^2_{x=S_i,t} + 36\frac{P^{ACL}_{H_2O}}{P_{sat}}\Big|^3_{x=S_i,t} \tag{28}$$

Lastly, two boundary conditions for the mass balance of chloride anions in the agglomerate have to be defined. The first condition is that the flux of this species in the center of the agglomerate is zero due to its assumed spherical structure:

$$J^{\mu}_{HCl_{(aq)}}(r = 0) = 0 \tag{29}$$

The second boundary condition concerns the concentration of HCl_{aq} at the surface of the agglomerates. As stated in the assumptions, a vapor/liquid equilibrium (VLE) between the HCl in its gaseous state within the CL and its dissolved state at the agglomerate surface is assumed. Since there is no sufficient experimental data available for the absorption of HCl in Nafion, the water and Nafion within the agglomerate is assumed to be homogenous, just like in the treatment of the membrane. The presence of the polymer is assumed to not influence the VLE and hence simply reduces the volume concentration of water and the absorbed $HCl_{(aq)}$. Due to the acidity of Nafion, it is likely that in reality the presence of the sulfonic acid groups does influence the VLE so that the absorption of gaseous HCl in Nafion should be subject of future research. The porosity of the agglomerate is determined by the volume of Nafion relatively to the total volume including the carbon support and the platinum catalyst. This presupposes that the volume of the agglomerate is not changing significantly with its water content, an assumption that is also made in various other models [46,47]. Due to the strongly non ideal nature of the system, it is not possible to employ Henry's law as oftentimes done for the ORR [42,46]. Hence, fit functions were generated to correlate the equilibrium mole fraction of chloride anions to the HCl partial pressure based on experimental data from Ref. [48] for temperatures of 25, 40, 50, 60, 70, 80 and 90 °C. Furthermore, a function was included in the code that linearly interpolates between these temperatures to enable the simulation to be carried out at any temperature in the interval of 25–90 °C. The fit functions for the mentioned temperatures are included in the supplemental information together with a graphical depiction of the data and fits.

For correlating the activity coefficient of chloride anions in water with their mole fraction, the same procedure was followed, employing experimental data from Cerquetti et al. [49], with the sole exception that the temperature of 90 °C was omitted due to a lack of experimental data. More details are given in the supplemental information.

2.5. Model parameters

Table 1 summarizes all model parameters employed in the simulation. The only two parameters that do not stem from previous literature are the reaction rate constant and the equilibrium constant for the adsorption of chloride ions to the platinum surface according to equation (15). The latter constant predominantly shifts the potential-current curve towards lower or higher potentials. Hence, it can be obtained directly by comparing the experimental U–I curve with the one obtained from the proposed model and changing K_0 so that the both are not parallel to each other but align. The reaction rate constant k_A can be approximated directly from the experimentally determined reaction limited current in the work of Martínez et al. [20] utilizing

Table 1
Model parameters implemented in the reactor simulation.

Parameter	Symbol	Value	Unit
Temperature	T	40 and 60	°C
Rate constant of Tafel step	k_A	$k_{A,40^\circ C} = 8.8435 \cdot 10^3 k_{A,60^\circ C} = 1.239 \cdot 10^4$	$\frac{mol}{m^3 s}$
Porosity CL	ε_{CL}	0.6	
Porosity GDL [9]	ε_{GDL}	0.75	
Nafion fraction agglomerate	$f_{N,agg}$	0.44	
Anode Gas chamber pressure	p_{tot}^{GC}	100000	Pa
Gas phase permeability [50]	$k_{eff,g}$	$1.56 \cdot 10^{-15}$	m^2
Viscosity [51]	$\mu_g \approx \mu_{HCl}$	$\mu_{HCl} = (-9.188 + 0.555T - 0.00011T^2)10^{-7}$	Pa s
Equilibrium constant chloride adsorption/desorption	K_0	$K_{40^\circ C} = 1.49 \cdot 10^{-7} K_{60^\circ C} = 8.51 \cdot 10^{-7}$	$\frac{m^3}{mol}$
Diffusion coefficient of hydrochloric acid in Nafion [28]	$D^{\mu}_{HCl_{(aq)}-H_2O}$	$1.2 \cdot 10^{-11}$	$\frac{m^2}{s}$
Agglomerate radius [42]	R	200	nm
GDL thickness [9]	L_{GDL}	400	μm
Thickness ACL [52]	L_{ACL}	10	μm
Thickness Membrane [20]	L_M	170	μm
Electrode area [20]	A_{ACL}	$2.3 \cdot 10^{-4}$	m^2
Volumetric flow rate of HCl at standard temperature and pressure (STP) [20]	$\dot{V}_{HCl}$	$8.33 \cdot 10^{-6}$	
Pre-factor, Diffusion coefficient of water in Nafion [31]	D_W^0	$2.1 \cdot 10^{-7}$	$\frac{m^2}{s}$
Density of dry membrane [53]	ρ_M	2000	$\frac{kg}{m^3}$
Equivalent weight of membrane [53]	EW	1.1	$\frac{kg}{mol}$
Drag coefficient membrane	ξ	3.5 at full membrane hydration	

$$k_A = \frac{j_{limit}}{2F(1-\varepsilon_{CL})L_{ACL}} \tag{30}$$

This relation is based on the assumption that at the experimentally observed reaction-limited current, the surface coverage is approximating values of one on the surface of the agglomerate and throughout the whole agglomerate itself. The first assumption is justified by the fact that the limiting behavior is induced by a saturation of catalyst sides so that the Tafel step is not further accelerated with an increase in the anode overpotential. The latter assumption is justified by the simulation results indicating that the effectiveness factor is essentially 1 under the experimental conditions of Martínez et al. [20] as shown in section 3.3.

Since the highest current densities investigated in the experiments of Martínez et al. [20] are still slightly below the reaction-limited current, they have to be approximated by an extrapolation of the data. Certainly, a more precise method would be to fit the simulative polarization curve to the experimental one with the reaction rate as a fit parameter employing a least-squares method. However, the approach of approximating the rate constant from the reaction-limited current and still being able to reproduce the experimental data further supports and validates the hypothesis of this work that the Tafel step is the reason for the observed limiting behavior, which is why the reaction rate constant is not systematically treated as a fitting parameter as outlined above in this work.

The differential equations discussed in the previous sections are solved in MATLAB R2015b based on the finite volume differentiation scheme within the GDL, the agglomerate and the membrane, employing 10 discretization cells in each case.

3. Results and discussion

3.1. Discussion of the current-voltage curves and the reaction limited current

In the following, the expression for the reaction rate introduced in section 2.3 is derived based on a discussion of the possible reaction pathways displayed in equation (17)–(19). Subsequently, the experimental and simulative polarization curves, including the observed limiting behavior, are discussed based on these insights.

As a first step in the determination of the reaction pathway, two Tafel plots from the work of Martínez et al. [16,20] are briefly discussed, one in which the data was corrected for what the authors believed to be mass transfer resistance (please see Fig. 5.4 in Ref. [20]) and one with raw, uncorrected experimental data (please see Fig. 6 in Ref. [16]). The latter one shows the Tafel slope approaching infinity at high current densities. Furthermore, the limiting current varies strongly for the different investigated catalyst systems and loadings. If a mass transfer limitation was at cause, one would expect the limiting current to be mostly uninfluenced by the catalyst loading and materials. As further discussed in section 3.2 and 3.3, the model of the present work supports these findings by showing that there is neither a mass transfer limitation in the gas phase transport of HCl in the anode GDL, nor the agglomerates of the anode catalyst layer.

In light of this, a clear discrimination of mechanism B, as shown in equations (17) and (19), is now possible as this reaction pathway would lead to Tafel slopes of 39–131 mV dec^{-1} depending on the overpotential [20]. Also the previously mentioned chloronium pathway is not able to explain the observed infinite Tafel slope, since the rate determining step is electrochemical [40]. However, the purely chemical step in Mechanism A would lead to the observed infinite Tafel slope at high overpotentials. Hence, for the present system and catalyst, the recombination reaction in mechanism A appears to be the logical reaction sequence.

Assuming a pre-equilibrium of the adsorption and desorption of chloride anions (eq. (17)) leads to the following expression for the current density j^{μ}

$$j^{\mu} = 2Fr_A = 2k_A\Theta^2 e^{\frac{2\alpha g\Theta}{RT}} \tag{31}$$

With Θ being the surface coverage of Pt–Cl species and g the rate of change of the free energy of adsorption with the surface coverage. If the reverse reaction is considered as well, equation (31) changes to:

$$j^{\mu} = 2k_A\Theta^2 e^{\frac{2\alpha g\Theta}{RT}} - 2k_{-A}(1-\Theta)^2 e^{\frac{-(1-\alpha)g\Theta}{RT}} p_{Cl_2} \tag{32}$$

Based on the assumption of a pre-equilibrium in equation (17), the surface coverage can be calculated utilizing the following expression for the Frumkin isotherm:

$$\frac{\Theta}{1-\Theta} e^{\frac{2\alpha g\Theta}{RT}} = K_0 a_{Cl^-} e^{\frac{\eta_A F}{RT}} \tag{33}$$

While in many publications this equation is simplified by assuming certain intervals for Θ in order to obtain an analytical solution [38], the complete equation is solved numerically in the present work during every iteration of the simulation, and the so obtained surface coverage is employed in the expression for the current density (eq. (32)). This ensures validity of the obtained solution for all possible values of the surface coverage.

Regarding the nature of active sites it should be noted that under the experimental conditions of Martínez et al. [20], the presence of platinum oxide species is to be expected, so that the reaction largely takes place via Cl• species that are adsorbed on the platinum oxide surface [38]. In the present work it is assumed that the amount of active sites available for the adsorption of chloride species stays constant in the investigated potential region, regardless of their nature, something that should be investigated in more detail in the future.

In the following, the experimental polarization data of Martínez et al. [20] is compared to the one obtained from simulations with the presented model for two different temperatures of 40 and 60 °C. The simulation results in Fig. 2 were obtained under the assumption of a Langmuir isotherm, i.e. $g = 0$ in equations (32) and (33). Assuming that the back reaction is only relevant at low overpotentials and hence low surface coverages so that $1 - \Theta \approx 1$, the current density can be expressed as follows by combining equations (32) and (33) and by further presuming the current density to be zero at the equilibrium potential:

$$\begin{aligned} j^{\mu} &= 2Fk_A \left(\frac{K_0 a_{Cl^-}}{1 + K_0 a_{Cl^-} e^{\frac{F\eta_A}{RT}}} \right)^2 e^{\frac{2F\eta_A}{RT}} - 2Fk_{-A} p_{Cl_2} \\ &= 2Fk_A \left(\frac{K_0 a_{Cl^-}}{1 + K_0 a_{Cl^-} e^{\frac{F\eta_A}{RT}}} \right)^2 e^{\frac{2F\eta}{RT}} \left(1 - e^{\frac{-2F\eta_A}{RT}} \right) \end{aligned} \tag{34}$$

Good agreement with the experimental data, especially at high overpotentials, could also be obtained with values of $g > 0$, i.e. employing the full Frumkin isotherm. However, the results employing a Langmuir isotherm showed better agreement with the experimental data at low and intermediate overpotentials, so that $g = 0$ was fixed in all simulations following from here on.

A comparison of experimental and simulation results in Fig. 2 shows good agreement over the whole interval of current

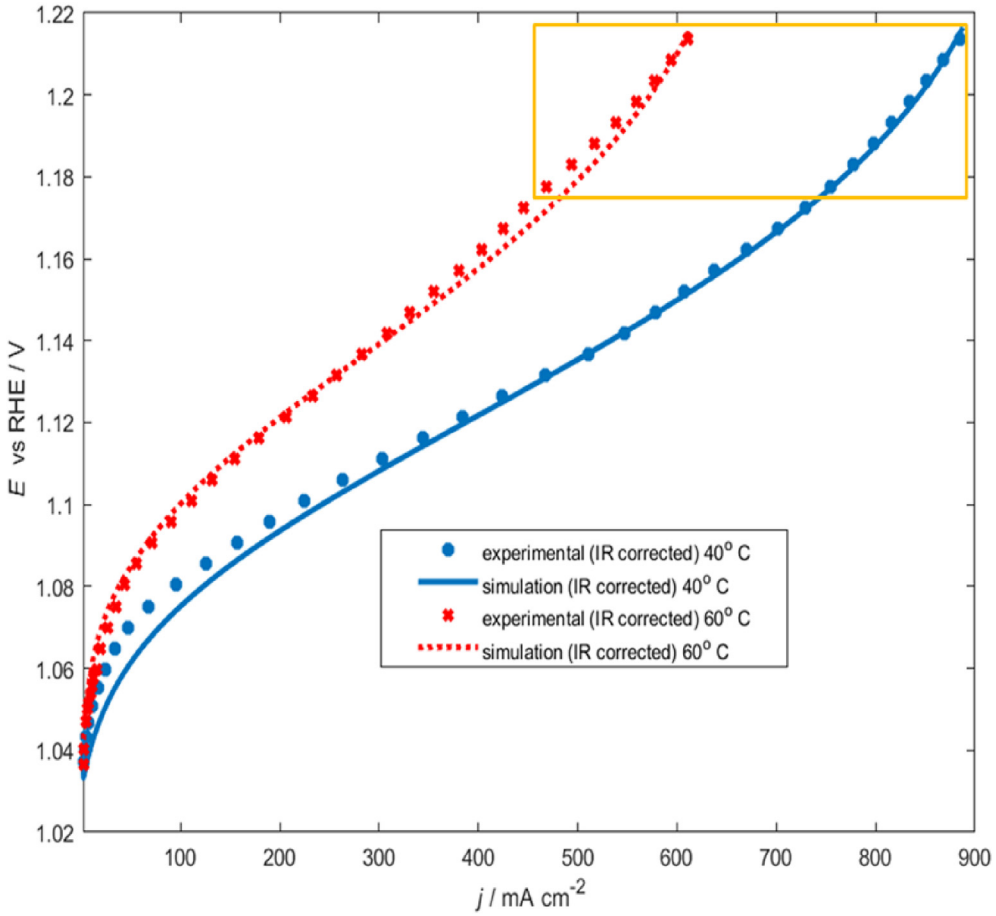

Fig. 2. Experimental polarization data from Ref. [20] in comparison with simulation data obtained with the presented model for 40 and 60 °C. The experimental data is corrected for ohmic resistance and expressed on the scale of a reference hydrogen electrode. The orange box visualizes the onset of the limiting behavior. (For interpretation of the references to colour in this figure legend, the reader is referred to the Web version of this article.)

densities without any model parameter being treated as an independent fitting parameter. The slight disagreement that is observable at higher current densities for the 40 °C case and at lower current densities for 60 °C case could be due to various reasons. First, it was assumed that the electrochemically active surface area (ECSA) is independent of the water content in the ACL or membrane. Zhu et al. [54] however, amongst others, propose that the ECSA however is sensitive to the membrane water content and relative humidity in the cell. Since these change over the interval of current densities considered in the present work, a better agreement would certainly be achieved if the ECSA was fitted to the water content as in Ref. [54]. However, as stated in previous sections, the authors refrained from increasing the amount of fitting parameters in the present work in order to obtain physically meaningful and realistic results. Second, further uncertainties lie in the water transport through the membrane being influenced by the presence of HCl, which, due to the lack of consistent data as discussed in detail in section 2.2, can currently only be partly taken into account. Third, the agglomerate size, which was extracted from the previous literature [42], does pose an additional uncertainty, even if of relatively minor influence as shown in section 3.3. Taking into account the above mentioned uncertainties, the nevertheless good agreement between the experimental and simulated polarization curves strongly supports the major hypothesis of a reaction- instead of a mass-transfer-limited current. As Fig. 3 demonstrated, the surface coverage approaches values of 1 at the highest current densities, justifying, together with the high effectiveness factor discussed earlier in this section, the approach of estimating the rate constant as delineated in section 2.5.

3.2. Mass transfer in the GDL

In the following, the mass transfer resistance is analyzed in detail to ensure that the observed limiting behavior is indeed a kinetic and not a mass transfer limitation. As discussed in the introduction of this article, the major contributions are expected to come from the mass transfer within the GDL and within the agglomerates. The concentration gradient within the porous catalyst layer can be assumed to be markedly smaller [36], since the CL in the experiments of Martínez et al. [16,19,20] is about 40 times thinner than their GDL.

The experimentally observed limiting behavior at a temperature of 60 °C is starting at current densities between 700 and 800 mA/cm^2. Fig. 4 depicts the mole fraction of HCl, water and chlorine throughout the whole thickness of the GDL at a current density of 800 mA/cm^2, where severe mass transfer limitations should be visible, if the limiting behavior was a consequence of slow mass transfer, as assumed by Martínez et al. [20].

While there certainly is a non-negligible concentration gradient of HCl in the GDL, it cannot explain the observed limiting behavior. This becomes especially clear when looking at the activities of the aqueous hydrochloric acid on the agglomerate surface that correspond to the gas phase concentration of HCl in the gas chamber ($L = 0$ in Fig. 4) and at the end of the GDL ($L = 400\ \mu$m). Due to the steep vapor-liquid equilibrium (VLE) curve of HCl/H_2O, the influence of the observed pressure gradient on the activity of the aqueous hydrochloric acid on the agglomerate surface is strongly reduced, as can be easily comprehended when looking at the VLE data given in the supplemental section. This further mitigates the influence of mass transport resistances in the GDL on the overall reactor performance.

3.3. Mass transfer and catalyst utilization within the agglomerates

After showing that the mass transfer resistance of the GDL is not responsible for the observed limiting behavior, the mass transfer within the agglomerate is investigated. A well-known coefficient for relating reaction kinetics to mass transfer within a porous particle is the effectiveness factor η, which can be calculated according to equation (35) [55]. The effectiveness factor is defined as the ratio of the amount of the reactant converted within the agglomerate to the amount that would have been converted if the same conditions that are present on the agglomerate surface prevailed throughout the whole agglomerate [55].

$$\eta = \frac{\iiint V_{agg} r dV}{V_{agg} r|_{surf}} = \frac{ag_i^{\mu}}{ag_{HCl_{(aq)}}^{\mu}\left(c = c_{surf}\right)} \tag{35}$$

The effectiveness factor as a function of the current density at a temperature of 60 °C is depicted in Fig. 5. The graph clearly underlines that the mass transfer resistance within the catalyst layer is significantly smaller compared to the kinetic resistance over the

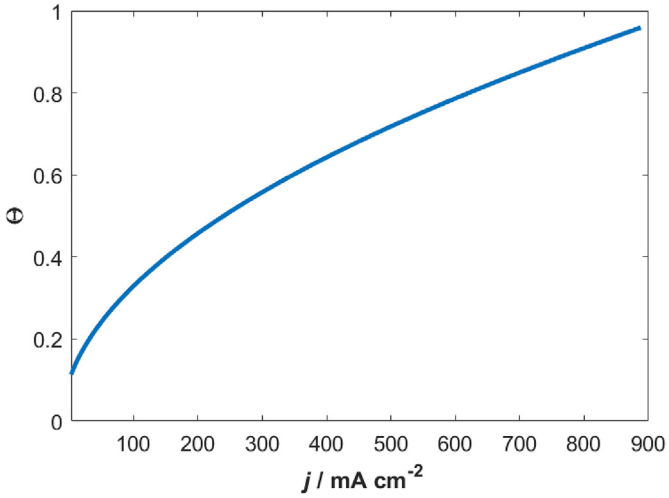

Fig. 3. Surface coverage under the conditions present at the surface of the agglomerates as a function of current density at 60 °C.

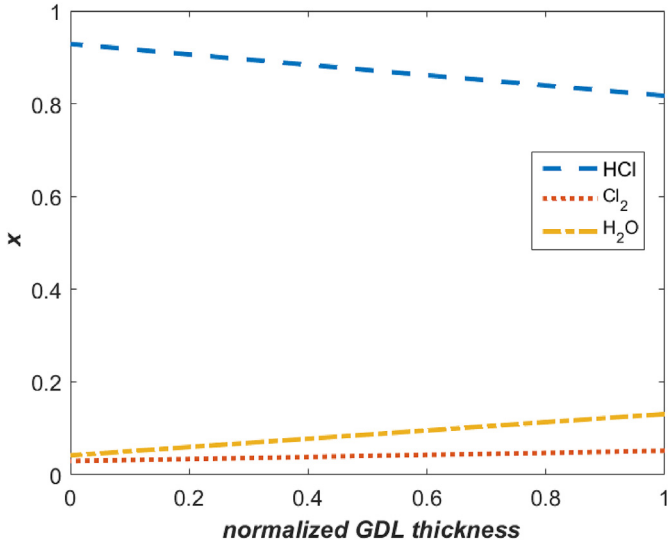

Fig. 4. Mole fractions of HCl, Cl_2 and H_2O over the normalized thickness of the AGDL at a current density of 800 mA/cm^2. The anode gas channel is located at a normalized thickness of zero.

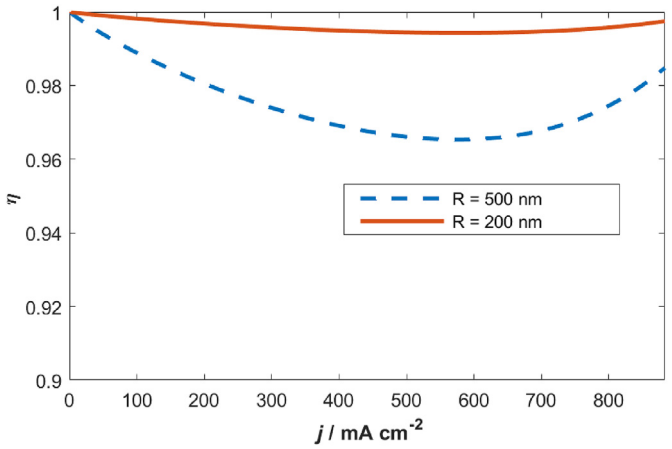

Fig. 5. Effectiveness factor for agglomerates with two different radii of 200 nm (red) and 500 nm (blue) in dependence of the current density of the reactor. (For interpretation of the references to colour in this figure legend, the reader is referred to the Web version of this article.)

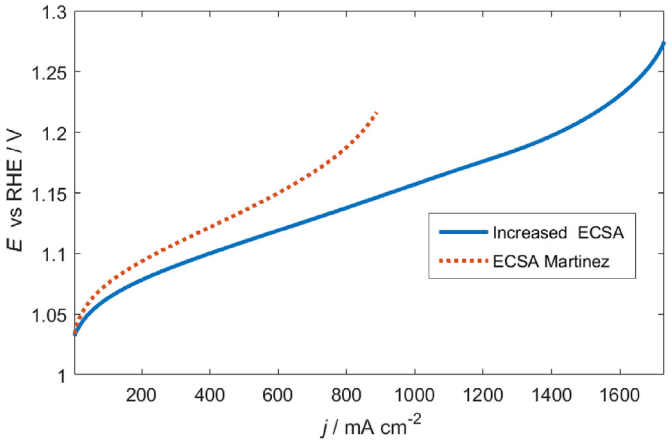

Fig. 6. Simulated polarization curves for the standard loading of 0.5 mg Pt/cm^2 and 1 mg Nafion/cm^2 (red dotted line) and an increased loading corresponding to a doubling of the active catalyst area (blue straight line). (For interpretation of the references to colour in this figure legend, the reader is referred to the Web version of this article.)

whole investigated interval of current densities. The decrease of the effectiveness factor with increasing current density is due to the acceleration of the reaction that comes with higher overpotentials coupled to higher current densities. Since the size of the agglomerates was adopted from Ref. [42] and its actual value for the MEA employed by Martínez et al. [20] is not precisely known, the effectiveness factor for a 2.5 times bigger agglomerate, $R = 500\ nm$, is also included in Fig. 5. Even for this increased agglomerate sizes, the mass transfer resistance is clearly smaller than the one due to the reaction kinetics. This stands in an interesting contrast to studies of the ORR in PEMFCs [56] and can be explained with the high concentration of $HCl_{(aq)}$ at the agglomerate surface which is 3 orders of magnitudes higher than the one for oxygen [20]. The reason for the increase in the effectiveness factor after reaching a minimum at 400−500 mA/cm^2, is that the overpotential rises strongly as the reaction limited current is reached. When looking at equation (33), it becomes obvious that at high potentials, the surface coverage approaches one. Hence, even though the activity of chloride anions within the agglomerate is declining with an increasing current density, the high overpotential increases the surface coverage more strongly so that it approaches values of one throughout the whole agglomerate, leading to the observed increase in the effectiveness factor. At significantly higher current densities, when mass transfer resistances in the agglomerate are becoming significant, the effectiveness factor decreases again. However, these mass transfer limitations only become relevant at current densities far beyond the reaction limited current density for the catalyst loading investigated by Martínez et al. [20].

Based on these insights it can be concluded that the observed limiting behavior is purely kinetic. The mass transfer resistances, discussed in section 3.2 and 3.3, certainly reduce the chloride ion activity in the agglomerates. As equation (33) shows, this leads to a slight increase in the overpotential in order to maintain the according surface coverage at any given current density. The reaction-limited current however is not influenced by this and only depends on the ECSA and the potential independent rate constant, summarized in k_A.

3.4. Deriving reactor optimization strategies

Finally, reactor optimization strategies based on the above discussed insights and model are discussed. In most of their experiments, Kuwertz et al. [9] employed a so called “standard loading” of 1 mg/cm^2 Pt and 0.5 mg/cm^2 Nafion. Martínez [20] however, proposed an optimized loading for the anode of 0.5 mg Pt/cm^2 and 1 mg Nafion/cm^2 and their experiments, which were used for validating the model in the present work, are based on this optimized loading.

Martínez’ et al. [20] approach of raising the Nafion content is justified by experiments showing that increasing the Nafion content at constant Pt loading lead to a significant increase in the reaction limited current density and a lower overpotential in the whole measured interval compared to the standard loading [20]. This can be attributed to the fact that the higher Nafion loading increases the amount of Pt particles in contact with the electrolyte and hence also the number of active sites, which turned out to be critical for the reactor performance based on the simulation results of the present work.

However in light of the new insights of this work, it is not recommended, especially if operation at high current densities is desired, to reduce the platinum loading. Experiments of Martínez et al. showed that the reaction limited current could be increased from ca 600 mA/cm^2 at 0.5 mg Pt/cm^2 to 800 mA/cm^2 at 1 mg Pt/cm^2 while keeping the Nafion loading constant at 0.5 mg/cm^2. This is again in good agreement with the insights of the present work, since the reaction limited current is expected to increase proportionally with the amount of active sites if the surface reaction is indeed the limiting factor. The most feasible strategy is hence, to increase both, the Nafion and Pt loading in the catalyst layer in order to further increase the ECSA. While this would also increase the thickness of the catalyst layer, the modeling results proved that mass transfer resistances are not significantly impeding the reactor performance. For this reason, the simulation was repeated with a 2 times higher amount of active sites, as it can be achieved with a thicker CL, and the results are graphically depicted in Fig. 6.

As expected, the overpotential over the whole current density regime is clearly reduced and the reaction limited current increases by a factor of ca. 2. While an increased Pt loading comes with higher investment costs for an industrial reactor, it has to be considered that the impact in the energy consumption of the reactor is significant. At a current density of only 400 mA/cm^2, the anode potential is reduced by 22 mV as a consequence of doubling the amount of active sites. Bechtel et al. [6] investigated the exergy demand of an industrial plant for the gas phase electrolysis of HCl

employing an ODC based on a MDI plant of BASF SE in Antwerp, Belgium. The operating current density was assumed to be 400 mA/cm^2 since in the full cell employing an ODC, several limiting effects are not allowing for operation at much higher current densities at the current state. A more detailed discussion about this can be found elsewhere [7]. The savings of 22 mV on the anode side are equivalent to savings in the electrical energy demand of the rector of $5{\cdot}10^6$ kWh per year for this industrial example plant. This translates to an annual cost reduction of 500000 € assuming a typical electricity price in Germany of ca 10 ct/kWh [57]. Furthermore, if the reactor can be operated at higher current densities, the size of the reactor, and therefore also the amount of catalyst, can be proportionally decreased, which dampens the effect of a higher platinum loading on the investment costs.

4. Summary

In the present work, a detailed reactor model of the gas phase oxidation of HCl is presented. None of the model parameters were systematically fit to experimental data; the only two parameters that were not extracted from previous literature but followed intrinsically from the experimentally determined OCV and the reaction-limited current were the reaction rate constant and the equilibrium constant for the adsorption and desorption of chloride anions on the catalyst surface. The model exhibited excellent agreement with previous experimental data, demonstrating that the experimentally observed limitations are due to the rate-determining Tafel step in the microkinetic mechanisms and that mass-transfer limitations are not the expected cause of performance limitations. Since the reaction limited current is at 400–950 mA/cm^2, depending on the reactor temperature, it also poses an important bottleneck in the performance of the overall electrolysis cell employing an ODC and not only the half-cell reaction itself, if operations at these current densities are desired. Hence, a new optimization strategy is proposed and first simulations show a significant potential for energetic and financial savings in an industrial application of the process.

Funding

This research did not receive any specific grant from funding agencies in the public, commercial, or not-for-profit sectors.

Acknowledgement and Affiliation

The author Simon Bechtel is also affiliated to the International Max Planck Research School (IMPRS) for Advanced Methods in Process and Systems Engineering, Magdeburg, Germany. The authors would like to thank Jennifer Uebbing for helpful discussions.

Appendix A. Supplementary data

Supplementary data to this article can be found online at https://doi.org/10.1016/j.electacta.2019.134780.

List of symbols

Symbol	Description	Unit
T	Temperature	°C
k_A, k_{-A}	Rate constants, Tafel step	$\frac{mol}{m^3 s}$
ε_{CL}	Porosity CL	
ε_{GDL}	Porosity GDL [9]	
$f_{N,agg}$	Nafion fraction agglomerate	
p_{tot}^{GC}	Gas channel pressure	Pa
$k_{eff,g}$	Gas phase permeability [50]	m^2
$\mu_g \approx \mu_{HCl}$	Viscosity [51]	Pa s
K_0	Equilibrium constant chloride adsorption/desorption	$\frac{m^3}{mol}$
$D^{\mu}_{HCl_{(aq)}-H_2O}$	Diffusion coefficient of hydrochloric acid in Nafion [28]	$\frac{m^2}{s}$
R	Agglomerate radius [42]	nm
L_{GDL}	GDL thickness [9]	µm
L_{ACL}	Thickness ACL [52]	µm
L_M	Thickness Membrane [20]	µm
A_{ACL}	Electrode area [20]	m^2
$\dot{V}_{HCl}$	Volumetric flow rate of HCl at STP [20]	$\frac{m^3}{s}$
$\dot{V}_{in}$ and $\dot{V}_{out}$	Volumetric flow rate entering and leaving the reactor	$\frac{m^3}{s}$
D_W^0	Pre-factor, Diffusion coefficient of water in Nafion [31]	$\frac{m^2}{s}$
$D_W(\lambda_M)$	Diffusion coefficient of water in Nafion	$\frac{m^2}{s}$
ρ_M	Density of dry membrane [53]	$\frac{kg}{m^3}$
EW	Equivalent weight of membrane [53]	$\frac{kg}{mol}$
ξ	Drag coefficient membrane	
K_M	Drag constant membrane	
κ_M	Ionic conductivity membrane	$\frac{S}{m}$
$\Delta\Phi_M$	Potential loss membrane	V
λ	Membrane water content	
c_W	Concentration of water in membrane	$\frac{mol}{m^3}$
α	Anodic transfer coefficient for the HClOR	
η_A	Overpotential Anode	V
E	Electrode potential vs SHE	V
E_{OCP}	Open circuit potential	V
P_i	Partial pressure of species i	Pa
P_{sat}	Water vapor pressure	Pa
j	Current density	$\frac{mA}{cm^2}$
j_{limit}	Limiting current density	$\frac{mA}{cm^2}$
Θ	surface coverage of Pt–Cl species	
D_{iM}^{eff}	Knudson diffusion coefficient of species i	$\frac{m^2}{s}$
D_{ij}^{eff}	Maxwell-Steffan diffusion coeffcients	$\frac{m^2}{s}$
$\overline{D_{ij}}_{eff}$	Diffusion coefficients for the inverted solutions of the Max well-Steffan equations (please see supplemental information)	$\frac{m^2}{s}$
g	Rate of change of the free energy of adsorption with coverage	$\frac{J}{mol}$
C_D^L	Double layer capacity	$\frac{\mu F}{cm^2}$
a_{Cl^-}	Activity of chloride anions	$\frac{mol}{m^3}$
η	Effectiveness factor agglomerates	
c_{surf}	Concentration of chloride anions on the surface of the agglomerates	$\frac{mol}{m^3}$

References

[1] M.F. Sonnenschein, Polyurethanes: Science, Technology, Markets, and Trends, 2014, https://doi.org/10.1002/9781118901274.
[2] Chemistry beyond chlorine. https://www.degruyter.com/downloadpdf/j/ci.2015.37.issue-1/ci-2015-0119/ci-2015-0119.pdf. (Accessed 31 May 2019).
[3] Chlorine market worth. https://issuu.com/jswapn23/docs/chlorine_market_worth. (Accessed 10 November 2017).
[4] J. Pérez-Ramírez, C. Mondelli, T. Schmidt, O.F.-K. Schlüter, A. Wolf, L. Mleczko, T. Dreier, Sustainable chlorine recycling via catalysed HCl oxidation: from fundamentals to implementation, Energy Environ. Sci. 4 (2011) 4786, https://doi.org/10.1039/c1ee02190g.
[5] Hydrochloric acid electrolysis sustainable chlorine production. https://www.digitalrefining.com/data/literature/file/869775969.pdf. (Accessed 21 August 2018).
[6] S. Bechtel, T. Vidaković-Koch, K. Sundmacher, Novel process for the exergetically efficient recycling of chlorine by gas phase electrolysis of hydrogen chloride, Chem. Eng. J. 346 (2018) 535–548, https://doi.org/10.1016/

j.cej.2018.04.064.
[7] S. Bechtel, Z. Song, T. Zhou, T. Vidaković-Koch, K. Sundmacher, Integrated process and ionic liquid design by combining flowsheet simulation with quantum-chemical solvent screening, Comput. Aided Chem. Eng. 44 (2018) 2167–2172, https://doi.org/10.1016/B978-0-444-64241-7.50356-6.
[8] S. Bechtel, T. Vidaković-Koch, K. Sundmacher, Energy-efficient gas-phase electrolysis of hydrogen chloride, Chem. Ing. Tech. 91 (2019) 795–808, https://doi.org/10.1002/cite.201800160.
[9] R. Kuwertz, N. Aoun, T. Turek, U. Kunz, Influence of PTFE content in gas diffusion layers used for gas-phase hydrogen chloride electrolysis with oxygen depolarized cathode, J. Electrochem. Soc. 163 (2016) F988–F997, https://doi.org/10.1149/2.0261609jes.
[10] S. Sui, X. Wang, X. Zhou, Y. Su, S. Riffat, C. jun Liu, A comprehensive review of Pt electrocatalysts for the oxygen reduction reaction: nanostructure, activity, mechanism and carbon support in PEM fuel cells, J. Mater. Chem. A. 5 (2017) 1808–1825, https://doi.org/10.1039/C6TA08580F.
[11] V. Mehta, J.S. Cooper, Review and analysis of PEM fuel cell design and manufacturing, J. Power Sources 114 (2003) 32–53, https://doi.org/10.1016/S0378-7753(02)00542-6.
[12] N. Ramaswamy, S. Mukerjee, Fundamental mechanistic understanding of electrocatalysis of oxygen reduction on Pt and non-Pt surfaces: acid versus alkaline media, Adv. Phys. Chem. (2012) 1–17, https://doi.org/10.1155/2012/491604, 2012.
[13] V. Tripković, E. Skúlason, S. Siahrostami, J.K. Nørskov, J. Rossmeisl, The oxygen reduction reaction mechanism on Pt(1 1 1) from density functional theory calculations, Electrochim. Acta 55 (2010) 7975–7981, https://doi.org/10.1016/j.electacta.2010.02.056.
[14] J.A. Trainham, C.G. Law, J.S. Newman, K.B. Keating, D.J. Eames, C.E. I du pont de Nemours and, US patent 5411641 A. https://patentimages.storage.googleapis.com/53/5b/44/362dd865f1e84a/US5411641.pdf, 1995. (Accessed 30 May 2019).
[15] D.J. Eames, Electrochemical conversion of anhydrous HCl to Cl[sub 2] using a solid-polymer-electrolyte electrolysis cell, J. Electrochem. Soc. 142 (2006) 3619, https://doi.org/10.1149/1.2048388.
[16] I.G. Martínez, T. Vidaković-Koch, R. Kuwertz, U. Kunz, T. Turek, K. Sundmacher, Analysis of a novel chlorine recycling process based on anhydrous HCl oxidation, Electrochim. Acta 123 (2014) 387–394, https://doi.org/10.1016/j.electacta.2014.01.050.
[17] W.H.J. Hogarth, J.B. Benziger, Dynamics of autohumidifed PEM fuel cell operation, J. Electrochem. Soc. 153 (2006) A2139, https://doi.org/10.1149/1.2344841.
[18] J. Zhang, H. Zhang, J. Wu, J. Zhang, The effects of temperature on PEM fuel cell kinetics and performance, Pem Fuel Cell Test. Diagnosis (2013) 121–141, https://doi.org/10.1016/b978-0-444-53688-4.00004-8.
[19] I.G. Martínez, T. Vidaković-Koch, R. Kuwertz, U. Kunz, T. Turek, K. Sundmacher, The kinetics of hydrogen chloride oxidation, J. Serb. Chem. Soc. 78 (2013) 2115–2130, https://doi.org/10.2298/JSC131119142G.
[20] I.G. Martínez, Hydrogen Chloride Electrolysis in a Polymer-Electrolyte-Membrane Reactor with Oxygen-Depolarized Cathode, 2015. Dissertation.
[21] R. Krishna, J. Wesselingh, Review article number 50 - the Maxwell-Stefan approach to mass transfer, Chem. Eng. Sci. 52 (1997) 861–911, 2019.
[22] F.B. Spingler, A. Phillips, T. Schuler, M.C. Tucker, A.Z. Weber, Investigating fuel-cell transport limitations using hydrogen limiting current, Int. J. Hydrogen Energy 42 (2017) 13960–13969, https://doi.org/10.1016/j.ijhydene.2017.01.036.
[23] I.V. Zenyuk, P.K. Das, A.Z. Weber, Understanding impacts of catalyst-layer thickness on fuel-cell performance via mathematical modeling, J. Electrochem. Soc. 163 (2016) F691–F703, https://doi.org/10.1149/2.1161607jes.
[24] R.J. Balliet, J. Newman, Cold start of a polymer-electrolyte fuel cell I. Development of a two-dimensional model, J. Electrochem. Soc. 158 (2011) B927, https://doi.org/10.1149/1.3592430.
[25] A. Sorrentino, T. Vidaković-Koch, R. Hanke-Rauschenbach, K. Sundmacher, Concentration-alternating frequency response: a new method for studying polymer electrolyte membrane fuel cell dynamics, Electrochim. Acta 243 (2017) 53–64, https://doi.org/10.1016/j.electacta.2017.04.150.
[26] M. Eikerling, Phenomenological theory of electro-osmotic effect and water management in polymer electrolyte proton-conducting membranes, J. Electrochem. Soc. 145 (2006) 2684, https://doi.org/10.1149/1.1838700.
[27] T.A. Zawodzinski, A comparative study of water uptake by and transport through ionomeric fuel cell membranes, J. Electrochem. Soc. 140 (1993) 1981–1985, https://doi.org/10.1149/1.2220749.
[28] T. Vidaković-Koch, I.G. Martínez, R. Kuwertz, U. Kunz, T. Turek, K. Sundmacher, Electrochemical membrane reactors for sustainable chlorine recycling, Membranes 2 (2012) 510–528, https://doi.org/10.3390/membranes2030510.
[29] S. Motupally, A.J. Becker, J.W. Weidner, Water transport in polymer electrolyte membrane electrolyzers used to recycle anhydrous HCl: I. Characterization of diffusion and electro-osmotic drag, J. Electrochem. Soc. 149 (2002) D69–D71, https://doi.org/10.1149/1.1464135.
[30] Z. Tang, R. Svoboda, J.S. Lawton, D.S. Aaron, A.B. Papandrew, T.A. Zawodzinski, Composition and conductivity of membranes equilibrated with solutions of sulfuric acid and vanadyl sulfate, J. Electrochem. Soc. 160 (2013) F1040–F1047, https://doi.org/10.1149/2.083309jes.
[31] T.F. Fuller, Solid-polymer-electrolyte Fuel Cells, 1992, https://doi.org/10.2172/7001224.
[32] T.E. Springer, T.A. Zawodzinski, S. Gottesfeld, Polymer electrolyte fuel cell model, J. Electrochem. Soc. 138 (1991) 2334, https://doi.org/10.1149/1.2085971.
[33] A.Z. Weber, J. Newman, Transport phenomena in polymer electrolyte membranes, J. Electrochem. Soc. 151 (2004) A311–A325, https://doi.org/10.1149/1.1639157.
[34] S. Motupally, A.J. Becker, J.W. Weidner, Tutorials in electrochemical engineering -mathematical modelling, in: R.F. Savinell, S.L. Scanlon, J.M. Fenton, J. Weidner (Eds.), Proceedings of the International Symposium of the Electrochemical Society, vols. 99–14, 1999.
[35] E.N. Balko, J.F. Mcelroy, A.B. Laconti, Halogen acid electrolysis in solid polymer electrolyte cells, Int. I. Hydrogen Energy 6 (1981) 577–587.
[36] H.A. Gasteiger, J.E. Panels, S.G. Yan, Dependence of PEM fuel cell performance on catalyst loading, J. Power Sources 127 (2004) 162–171, https://doi.org/10.1016/j.jpowsour.2003.09.013.
[37] B.V. Tilak, Kinetics of chlorine evolution—a comparative study, J. Electrochem. Soc. 126 (1979) 1343–1348, https://doi.org/10.1149/1.2129274.
[38] B.E. Conway, D.M. Novak, Electrocatalytic effect of the oxide film at Pt anodes on Cl2 recombination kinetics in chlorine evolution, J. Electroanal. Chem. 99 (1979) 133–156, https://doi.org/10.1016/S0022-0728(79)80243-0.
[39] G. Faita, G. Fiori, A. Nidola, Anodic discharge of chloride ions on Pt-Ir alloy electrodes, J. Electrochem. Soc. 117 (1970) 1333–1335, https://doi.org/10.1149/1.2407304.
[40] L.I. Krishtalik, Kinetics and mechanism of anodic chlorine and oxygen evolution reactions on transition metal oxide electrodes 26 (1980) 329–337, https://doi.org/10.1016/0013-4686(81)85019-0.
[41] E. Guerrini, V. Consonni, S. Trasatti, Surface and electrocatalytic properties of well-defined and vicinal RuO2 single crystal faces, J. Solid State Electrochem. 9 (2005) 320–329, https://doi.org/10.1007/s10008-004-0602-1.
[42] L. Xing, M. Mamlouk, K. Scott, A two dimensional agglomerate model for a proton exchange membrane fuel cell, Energy 61 (2013) 196–210, https://doi.org/10.1016/j.energy.2013.08.026.
[43] S. Calabrese Barton, Oxygen transport in composite mediated biocathodes, Electrochim. Acta 50 (2005) 2145–2153, https://doi.org/10.1016/j.electacta.2004.09.022.
[44] U. Krewer, T. Vidakovic-Koch, L. Rihko-Struckmann, Electrochemical oxidation of carbon-containing fuels and their dynamics in low-temperature fuel cells, ChemPhysChem 12 (2011) 2518–2544, https://doi.org/10.1002/cphc.201100095.
[45] M. Secanell, K. Karan, A. Suleman, N. Djilali, Optimal design of ultralow-platinum PEMFC anode electrodes, J. Electrochem. Soc. 155 (2008) B125, https://doi.org/10.1149/1.2806171.
[46] W. Sun, B.A. Peppley, K. Karan, An improved two-dimensional agglomerate cathode model to study the influence of catalyst layer structural parameters, Electrochim. Acta 50 (2005) 3359–3374, https://doi.org/10.1016/j.electacta.2004.12.009.
[47] A.A. Kulikovsky, Two-dimensional numerical modelling of a direct methanol fuel cell, J. Appl. Electrochem. 30 (2000) 1005–1014, https://doi.org/10.1023/A:1004086402501.
[48] R. Perry, S. Perry, D. Green, J. Maloney, Chemical Engineers' Handbook, seventh ed., 1997, https://doi.org/10.1021/ed027p533.1.
[49] A. Cerquetti, P. Longhi, T. Mussini, Thermodynamics of aqueous hydrochloric acid from the emf. of hydrogen-chlorine cells, J. Chem. Eng. Data 13 (1968) 458–461, https://doi.org/10.1021/je60039a001.
[50] A.Z. Weber, R.M. Darling, J. Newman, Modeling two-phase behavior in PEFCs, J. Electrochem. Soc. 151 (2004) A1715, https://doi.org/10.1149/1.1792891.
[51] A.K. Coker, E.E. Ludwig, Ludwig's Applied Process Design for Chemical and Petrochemical Plants, vol. 1, Elsevier Gulf Professional, 2007.
[52] R. Kuwertz, I.G. Martínez, T. Vidaković-Koch, K. Sundmacher, T. Turek, U. Kunz, Material development and process optimization for gas-phase hydrogen chloride electrolysis with oxygen depolarized cathode, J. Appl. Electrochem. 46 (2016) 755–767, https://doi.org/10.1007/s10800-016-0966-9.
[53] A. Kosuglu, A.Z. Weber, New insights into perfluorinated sulfonic-acid ionomers, Chem. Rev. 117 (2017) 987–1104, https://doi.org/10.1021/acs.chemrev.6b00159.
[54] M. Zhu, X. Xie, K. Wu, A.-U.-H. Najmi, K. Jiao, Experimental investigation of the effect of membrane water content on PEM fuel cell cold start, Energy Procedia 158 (2019) 1724–1729, https://doi.org/10.1016/J.EGYPRO.2019.01.401.
[55] R.J. (Ruud J. Wijngaarden, A. Kronberg, K.R. Westerterp, Industrial Catalysis: Optimizing Catalysts and Processes, Ch. 6, Wiley-VCH, 1998.
[56] W.K. Epting, S. Litster, Effects of an agglomerate size distribution on the PEFC agglomerate model, Int. J. Hydrogen Energy 37 (2012) 8505–8511, https://doi.org/10.1016/j.ijhydene.2012.02.099.
[57] Industry prices for electricity in Germany 2008-2017. https://www.statista.com/statistics/595803/electricity-industry-price-germany/. (Accessed 30 May 2019).